2012 NDIA GROUND VEHICLE SYSTEMS ENGINEERING AND TECHNOLOGY SYMPOSIUM
MODELING & SIMULATION, TESTING AND VALIDATION (MSTV) MINI-SYMPOSIUM
AUGUST 14-16, MICHIGAN

SIMULATION OF THERMAL SIGNATURE OF TIRES AND TRACKS

Tian Tang
Center for Advanced Vehicular Systems
Mississippi State University
Starkville, MS

Daniel Johnson
Emily Ledbury
Thomas Goddette
Sergio D. Felicelli*
Center for Advanced vehicular Systems
and Dept. of Mechanical Engineering
Mississippi State University
Starkville, MS

Robert E. Smith
CASSI Thermal and Signature Modeling Team
RDECOM-TARDEC
Warren, MI

ABSTRACT

Rubber is the main element of tires and the outside layer of tracks. Tire and track heating is caused by hysteresis effects due to the deformation of the rubber during operation. Tire temperatures can depend on many factors, including tire geometry, inflation pressure, vehicle load and speed, road type and temperature and environmental conditions. The focus of this study is to develop a finite element approach to computationally evaluate the temperature field of a steady-state rolling tire and track. The 3D thermal analysis software Radtherm was applied to calculate the average temperature of tread and sidewall, and the results of Radtherm agreed with ABAQUS results very well. The distributions of stress and strain energy density of the rolling tracks were investigated by ABAQUS as well. The future works were finally presented.

1. INTRODUCTION

Rubber is the primary component of tires and track outside layers. Rubber is a viscoelastic material and as such it shows hysteresis during cyclic loading, i.e., less energy is given back during unloading than was received during loading, the missing energy being dissipated as heat. The effect is more pronounced when the loading/unloading is done quickly, as in a high speed rolling tire. The prediction of the tire thermal signature requires the calculation of the surface temperature of the tire under vehicle operating conditions in the field. Tire temperatures can depend on many factors, including tire geometry, inflation pressure, vehicle load and speed, road type and temperature and environmental conditions. Tire heating can significantly affect the infrared (IR) signature of a vehicle. In an IR signature prediction model, accurate tire heat generation values are necessary to ensure accurate IR signature prediction.

In this paper, a finite element approach was developed to calculate the heat generation source within tires and tracks operating in several conditions, which is then used for thermal and infrared signature analysis. The analysis procedure of Radtherm was developed and the results were verified by ABAQUS.

2. HEAT GENERATION THEORETICAL BACKGROUND

Heat generation or energy loss of rubber is primarily due to internal hysteresis when the energy recovered from elastic deformation is less than the energy required to create elastic deformation [1]. Hysteresis is due to the viscoelastic nature of rubber, the primary component of tires. The experimental data shows that, for the speeds of 80 to 95 mph, hysteresis accounts for 90 to 95% energy losses, 2 to 10% of energy losses are from friction between the tire and the road, and air resistance accounts for 1.5 to 3.5% of losses [2]. For the purpose of this study, it is assumed that heat generation in the tire is created by the hysteresis of the rolling tire. Mechanical testing, specifically DMA testing, can be performed to determine the hysteresis of rubber. The work presented here uses a hysteresis value reported in Ref. [3].

Hysteresis can be defined as lost strain energy density divided by the total strain energy density [3] shown as:

$$H = \frac{U_{loss}}{U_{total}} \quad (1)$$

Strain energy is the potential energy stored during elastic deformation. Strain energy density is strain energy per unit volume. In this study strain energy density and hysteresis will be used to calculate the heat generated within a rolling tire. The total strain energy density that is calculated from the deformation module is multiplied with the hysteresis to find the lost strain energy density:

$$U_{loss} = H.U_{total} \quad (2)$$

The lost strain energy density is the energy that is not recovered after deformation which is assumed to completely contribute to internal heat generation in this study. In order to calculate the heat generation rate, the rotation rate of the tire or track wheel is needed. Frequency is defined as the velocity divided by the circumference of the rolling tire with the following equation:

$$f = \frac{V_L}{L_c} \quad (3)$$

$$L_c = 2\pi R \quad (4)$$

where V_L is the speed, L_c is the circumferential length of the rolling tire or track wheel, and R is the radius of the rolling tire or track wheel.

Once the frequency of the rolling tire or track wheel is found it is multiplied with the lost strain energy density to calculate the heat generation rate per unit volume (J/m^3) for each element.

$$\dot{q}_v = U_{loss} \cdot f \quad (5)$$

3. SIMULATION DETAILS

3.1. Simulation procedures of the temperature field of a steady rolling tire

The simulations of temperature fields of a steady-state rolling tire were accomplished by developing finite element mechanical and thermal models. The mechanical model was created using the Tire Wizard provided in Abaqus/Standard CAE. The size of a standard passenger tire (185/60 R15) was used for the simulations in this work. The simulation procedures are as follows:

1. Firstly, an axi-symmetric cross-section of a tire was created, as shown in Fig. 1, and the tire was inflated. The tire is assumed to be composed of rubber and body-ply whose material properties are listed in Table 1. Note that the rubber is characterized by the Mooney-Rivlin model while the body-ply is a linear elastic material. To facilitate the analysis, the tire was divided into Tread and Sidewall by the dash line as shown in Fig. 1. Only circumferential grooves were considered in this study.
2. Then, a half tire was created from the axisymmetric model using the revolve feature in the Tire Wizard as shown in Fig. 2. A static load is applied to the tire. The tire is in contact with the road which is modeled as a rigid surface. Pressure, load, and contact conditions are applied. The steady state transport function available in the Tire Wizard is used to evaluate the tire under free rolling conditions including the effects of friction. In this work a simplification to the axisymmetric tire geometry is made to the rolling model and the bead region that connects to the rim is not included. The steady state rolling analysis uses a mixed Eulerian/Lagrangian reference frame. The rigid body rotation is defined in an Eulerian reference frame and the deformation is measured using a Lagrangian method [4]. The steady state transport analysis model is used to calculate the elastic strain energy density (ESEDEN) of the model which is the U_{total} in Eqs. (1) and (2).
3. Finally, a 2D axi-symmetric thermal analysis is performed to study the temperature evolution in the tire due to heat generation. The thermal analysis mesh is identical to the cross section of the 3D tire mesh used for the deformation analysis. As a first approximation, continuum 2D axi-symmetric elements were used in a heat transfer analysis. Hence the analysis is not coupled with the mechanical simulation that was previously performed. The heat transfer coefficients are taken from the literature [1] and summarized in Table 2. The temperature is assumed to be 25 °C for both the ambient atmosphere and the road surface. The temperature inside the tire is assumed to be 38 °C. The thermal conductivities are assumed to be temperature-independent, as listed in Table 1. Fig. 3 shows the different surfaces where the described thermal boundary conditions have been applied.

Furthermore, the road is assumed to be rigid and the fluctuation of friction between the road and tire is assumed negligible. The friction coefficient between the rigid road ant the tire was taken as 0.5. Because of the steady-state rolling on a flat surface condition, the heat generation caused by friction was assumed negligible compared to that caused by hysteresis effects.

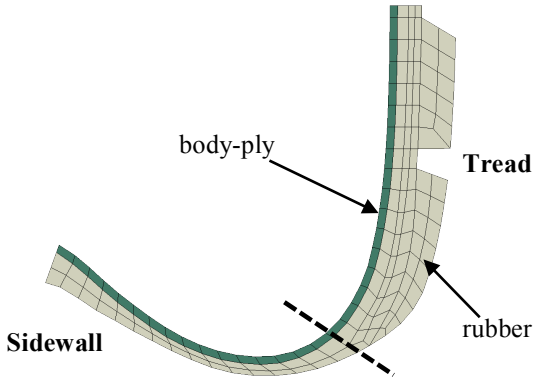

Fig. 1. The axi-symmetric cross-section of an inflated tire.

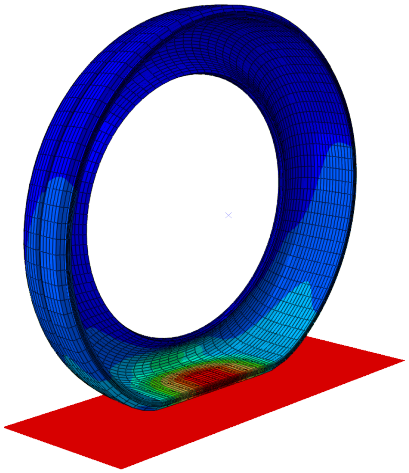

Fig. 2. The finite element half tire model was applied by inflation pressure, load, and contact condition.

Table 1. Material Properties used in this study.

Material	Rubber	Body-ply
Density (kg/m³)	1200	1200
Poison's Ratio		0.3
Young's Modulus (MPa)		500
Mooney-Rivlin Constants (MPa)	C_{10} = 0.8061 C_{01}= 1.805 D_1 = 0.01	-
Thermal conductivity (W/m °C)	0.293	0.293

Table 2. Heat transfer coefficients used for thermal boundary conditions in thermal module [1].

Boundary condition location	Heat transfer coefficient (W/m^2 °C)	Sink temperature (°C)
Tread/road	12000	25
Tread/air	16.18	25
Sidewall/air	16.18	25
Body-ply/cavity air	5.9	38
Liner/rim	88000	25

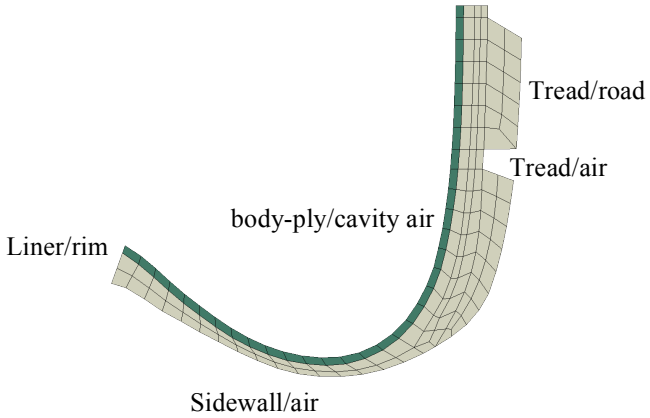

Fig. 3. Thermal boundary conditions for heat transfer analysis of tire.

3.2. Thermal Analysis for 3D Steady State Rolling Tire with RadTherm Software

Thermal analysis for three-dimensional (3D) steady state rolling tire was also performed with Radtherm software [5]. In this model, all three heat transfer modes, conduction, convection, and radiation, are taken into account. The geometry and meshing information are imported in the format of Nastran from Hypermesh. The thermal properties of each material and thermal boundary conditions are imported directly through the software interface. The heat generation due to the hysteresis effect during tire operation is obtained through deformation and mechanical models in the three-dimensional (3D) steady state rolling tire analysis with Abaqus. The correlations of heat generation as a function of tire operation parameters including pressure, speed, and load, are obtained through parameter studies. The heat generation is then imported to Radtherm through a user subroutine. In this model, the user input parameters for the tire thermal analysis include operation conditions (e.g. pressure, speed, load), tire type (e.g. geometry, rubber material), thermal properties of each material, and thermal boundary conditions.

3.2.1 Geometry and meshing

The three-dimensional (3D) tire geometry is created by Hypermesh, and then exported as Nastran format including geometry and mesh information with shell elements. The geometry file is then imported to the Radtherm software [5]. The tire geometry includes four different parts: ***rim, hub, tread,*** and ***sidewall.***

Parts with steel or Aluminum materials, such as rim and hub, are assigned as standard shell elements including front and back layers. Parts with rubber material, such as tread and sidewall, are assigned 2-layers shell elements including front, middle, and back layers. The heat generation in the rubber is assigned as heat rate in the middle layer.

3.2.2. Boundary conditions and thermal properties

The thermal boundary conditions and thermal properties of materials for each part are identical to those used in ABAQUS models. Different layers of each part are assigned as different boundary conditions. The tire is treated as a pure rubber material with given thermal properties, including thermal conductivity, specific heat, and density. Radiation heat transfer between parts and into the environment is taken into account. The view factors for the radiation heat transfer are calculated in Radtherm. Convective heat transfer is considered for both inside and outside the tire. A fluid node is applied to the air inside the tire, with given heat transfer coefficient and air temperature inside the tire. Since we only focus on steady-state temperature distribution, the fluid node inside the tire does not vary in pressure and temperature. Similarly, another fluid node is applied to the air outside the tire, with given heat transfer coefficient and environmental temperature. For the shell type element in Radtherm, only one element is assigned through the thickness of the tire. Therefore, the thickness of the element is the same as the thickness of the tire. The heat generation, called ***heat rate*** in Radtherm, is applied to the middle layer for each 2-layer shell element in the tread and sidewall. Except the heat rate, all boundary conditions and thermal properties are imported to Radtherm through the software interface.

The heat rate is imported through the user subroutine with a script module in Radtherm. The heat rate (W) is assigned to each element, instead of the whole part.

3.2.3. Heat rate calculation

The heat rate should be applied to each element in the parts with rubber material, including tread and sidewall. In this section, the heat rate for each part is calculated.

In the steady state rolling tire analysis, the cross section of the tire with road contact shows the maximum strain energy, as well as the maximum heat rate (W), due to the large deformation and hysteresis energy loss. Due to the symmetric nature of the steady state rolling tire analysis, the volumetric heat flux (W/m^3) at the cross section of the tire with road contact can be applied to the whole part of the 3D full tire in the thermal analysis.

The average strain energy density for each part (tread or sidewall) in the cross section of the tire with road contact is given by

$$\overline{E} = \frac{U}{V} = \frac{\sum_{i=1}^{n} E_i V_i}{V} (\mathrm{J/m^3}) \tag{6}$$

where U is the total strain energy for the part (tread or sidewall) in the cross section of the tire with road contact (J), V is the total volume of the part (m^3), n is the number of elements in the part, E_i is the strain energy density for each element in the part, and V_i is the volume for each element in the part. The strain energy density for each element in the cross section of the tire with road contact is obtained from the 3D steady state rolling tire analysis with Abaqus.

Note that the average strain energy density in the part (tread or sidewall) is a single value for the specific operation conditions (e.g. pressure, speed, load) and specific tire (e.g. material, geometry), calculated by the deformation and mechanical models with Abaqus. Through parameter studies, the correlations for average strain energy density in the part (tread or sidewall) can be obtained as a function of operation conditions (e.g. pressure, speed, load) for different types of tires.

The average volumetric heat flux for each element in the part (tread or sidewall) is calculated by

$$\dot{q} = \frac{H \cdot \overline{E} \cdot W}{2\pi R} (\mathrm{W/m^3}) \tag{7}$$

where R is the tire radius and H is the hysteresis loss factor of rubber material.

The average volumetric heat flux is applied to calculate the heat rate for each element in the part (tread or sidewall) of the 3D full tire model in Radtherm using the following equation:

$$q = \dot{q} \cdot A_i \cdot d (\mathrm{W}) \tag{8}$$

where A_i is the surface area of each element (m^2), d is the thickness of the element (m). For the shell type element in Radtherm, note that only one element is assigned through the thickness of the tire. Therefore, the thickness of the element is the same as the thickness of the tire.

3.3. Simulation procedures of track heating

3.3.1. Geometry and Mesh

The model was created by exporting four parts from the Pro-E/Creo assembly and then importing those parts into ABAQUS. These parts include the road wheel, the shoe, the backer, and the road pad as seen assembled in Figure 4. Because of the complicated geometries of some of these parts, tetrahedron elements were the only element type available for use. These simulations used first order tetrahedron elements for the meshing shown in Figure 5.

3.3.2. Loading and Boundary Conditions

Two types of loads were applied in this study as shown in Fig. 6. The first load was the weight of the tank applied to the road wheel. This load was applied by using a concentrated force at the center of the road wheel. Also, the track had a tension load that was applied in the center of the holes in the track. Both loads were 5000 lbf.

Two steps were used in this analysis, loading and rolling. In both steps, boundary conditions were applied to the track and the road wheel. For the loading step, the track was pinned at the bottom so that no displacements were taken place in all directions. The road wheel was fixed in all directions except for the vertical direction. For the rolling step, the road wheel was allowed to move in both the vertical and horizontal directions, and the linear velocity and angular velocity were applied to the road wheel.

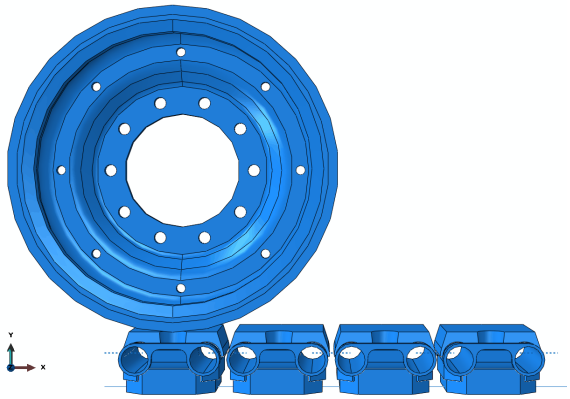

Fig. 4. Track geometry used in the analysis.

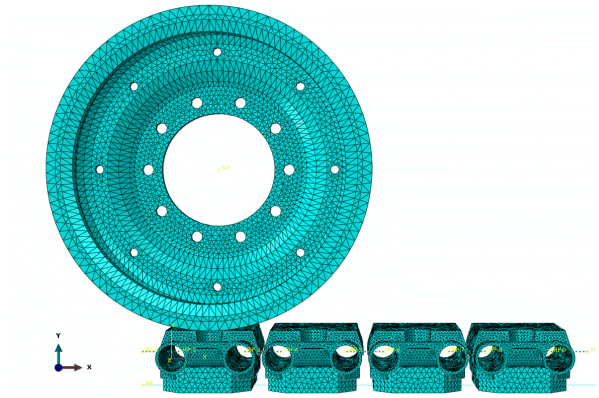

Fig. 5. Track mesh used in the analysis.

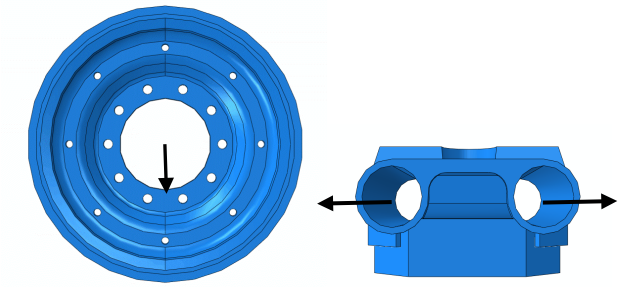

Fig. 6. Loads applied to the model.

The materials used in this study were steel and a hyper-elastic rubber. Generic steel was used for the steel components, and the hyper-elastic material was defined using Mooney-Rivlin constants. The properties of these materials are summarized in Table 3. These material properties were applied to different components of the model shown in Figure 7. The outer part of the road wheel, the backer, and the road pad all used the rubber properties, and the inner part of the road wheel and the shoe used the steel properties.

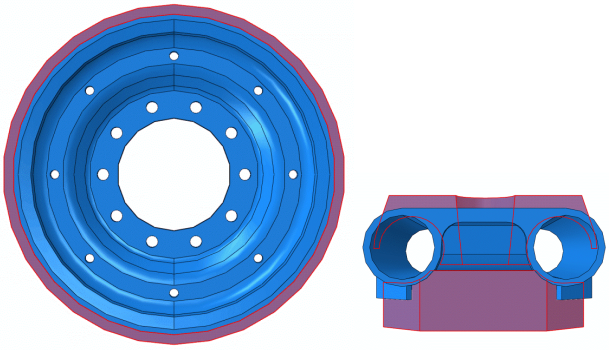

Fig. 7. Highlighted regions showing rubber components

Table 3. Material Properties used for the simulations of track heating models.

Material	Rubber	steel
Density ((lbf-s^2 / in^4)	1.12E-04	7.36E-04
Poison's Ratio		0.29
Young's Modulus (psi)		2.97E+07
Mooney-Rivlin Constants (psi)	C_{10} = 1.72E+04 C_{01}= -1.04E+04 D_1 = 2.07E-04	-

4. SIMULATION RESULTS AND DISCUSSIONS

This section presents (1) the predictions of temperature distribution of a steady-state rolling tire; (2) the Radtherm results of temperature field of a steady-state rolling tire; and (3) the distribution of strain energy density of track.

4.1. Finite element simulations of the temperature distribution of a steady-state rolling tire

The focus of this section is to analyze the coupled influences of the inflation pressure P and vehicle loading F. All simulation results were obtained at a constant velocity of V=80 km/h (22.2 m/s). Fig. 8, 9, and 10 show the contour plots of temperature distributions and the corresponding body heat flux calculated at various inflation pressure P=35, 50, and 70 psi and various loading F=3, 6, and 9 kN, respectively. Note that the body heat flux was directly calculated from the strain energy density using Eq. (5). As the loading is F=3 kN and 6 kN as shown in Fig. 7 and 8, the highest strain energy density and temperature are both located at the shoulder, while the high temperature area decreases as the inflation pressure P increases since higher inflation pressure results in less deformation in the rubber. When the loading was increased up to F=9 kN and the inflation pressure is P= 35 psi as shown in Fig. 9 (a-1) and (a-2), the most severe deformation occurs at the sidewall and the interface between the tread and sidewall such that the temperature of the sidewall next to the tread is the highest. As the inflation pressure was increased, the highest strain energy density and temperature moved to the shoulder.

The variations of the highest temperature with inflation pressure and loading are presented in Fig. 11. It can be observed that increasing the loading increased the highest temperature. The highest temperature increased slightly with the inflation pressure at the loading F=3 kN. However, the trend of the variation of the highest temperature changed as the loading was increased to 6 kN and 9 kN. The highest temperature decreased slightly with inflation pressure at the loading F=6 kN. In general, the influence of the inflation pressure on the highest temperature is not significant when the loading is not high such as 3 kN and 6 kN. When the loading was increased to 9 kN, the highest temperature decreased rapidly with the increase of the inflation pressure up to 50 psi and the influence of the inflation pressure increasing more than 50 psi is not high.

Fig. 12 shows the variation of the total averaged strain energy density with the inflation pressure and loading, which demonstrates that increasing the normal loading increases the deformation that the tire undergoes. Therefore, the variation of the total averaged temperature with the inflation pressures and loadings follows the same trend as shown in Fig. 13. The variations of the average temperature of the tread (T_tread) and sidewall (T_sw) with the inflation pressures and loadings were presented in Fig. 14. There is almost no difference between the T_tread and T_sw when the loading is F=3 kN and 6 kN. At high loading F=9 kN, the T_tread is much higher than T_sw at low inflation pressure. The difference between T_tread and T_sw decreases with the increase of the inflation pressure at F=9 kN.

4.2. Simulations of the average temperature of a steady-state rolling tire using Radtherm

To simulate the average temperature of a steady-state rolling tire using Radtherm software, we need to first obtain the correlations of average strain energy density of tread and sidewall as a function of tire operation parameters including inflation pressure **P**, speed **V**, and loading **F**. To this end, we calculated the strain energy density of a steady-state rolling tire at various **P**, **V**, and **F**. All simulation results are listed in Table 4. To more clearly clarify the variation trends of average strain energy density of tread and sidewall, the variation of the averaged strain energy density of tread ($\overline{ESE}_{Tread}$) and sidewall ($\overline{ESE}_{Sidewall}$) with the inflation pressures and loadings were plotted in Fig. 15 and 16, respectively. It can be seen that the variation trend of strain energy density with the inflation pressure is strongly dependent on the loading. According to the simulation results, the correlations of average strain energy density of tread and sidewall as a function of the tire operation parameters, inflation pressure **P**, speed **V**, and loading **F** can be expressed as:

$$\overline{ESE}_{Tread} = 0.00000307(\boldsymbol{P}-50)^2 + 0.0129 + 0.00357(\boldsymbol{F}-3) + 0.000075(\boldsymbol{V}-40) \quad \text{if } 4.5\text{kN} \geq \boldsymbol{F} \geq 3\text{kN}$$

$$\overline{ESE}_{Tread} = 0.0000029(\boldsymbol{P}-70)^2 + 0.0201 + 0.00257(\boldsymbol{F}-5) + 0.000075(\boldsymbol{V}-40) \quad \text{if } 6.5\text{kN} \geq F > 4.5\text{kN}$$

$$\overline{ESE}_{Tread} = -0.0002428\boldsymbol{P} + 0.000071207\boldsymbol{V} + 0.005778\boldsymbol{F} \quad \text{if } F > 6.5 \text{ kN}$$

$$\overline{ESE}_{SW} = 0.0126 + 0.000274(\boldsymbol{P} - 35) + 0.0042(\boldsymbol{F} - 3) + 0.000008(\boldsymbol{V} - 40) \quad \text{if F}\leq 5.5\text{kN}$$

$$\overline{ESE}_{SW} = 0.0288 + 0.0000036(\boldsymbol{P} - 50)^2 + 0.0106(\boldsymbol{F} - 6) - 0.00001(\boldsymbol{V} - 40) \quad \text{if } 7.5\text{kN}\geq \text{F} > 5.5\text{kN}$$

$$\overline{ESE}_{SW} = 0.0436 + 10^{-5}(P - 70)^2 + 0.0108(F - 8) - 0.00001(V - 40) \quad \text{if F=8 kN}$$

$$\overline{ESE}_{SW} = 0.0436 + 1.54 \cdot 10^{-5} \cdot (\boldsymbol{F} - 8) \cdot (\boldsymbol{P} - 70)^2 + 0.0108 \cdot (\boldsymbol{F} - 8) - 0.00001 \cdot (V - 40) \quad \text{if F}\geq 9\text{ kN}$$

To verify the simulation results of Radtherm, we also used ABAQUS to calculate the average temperature. Table 5 presents the predictions computed by ABAQUS and Radtherm. There is very good agreement between the simulation results obtained by both approaches. Fig. 17 and 18 show the contour plots of average temperature of the tread and sidewall of a steady-state rolling tire at **P**=35 psi, **V**= 80 km/h, **F**=3kN and **P**=35 psi, **V**= 80 km/h, **F**=9kN, respectively.

4.3. Simulations of the distribution of strain energy density of track

The results of this analysis are shown in Figures 19-21. In Fig. 19, the stress for the loading of the road wheel is shown. In Fig. 20, the elastic strain energy density (ESEDEN) for the beginning of rolling is shown, and the ESEDEN for the transition from the first pad to the second pad is shown in Fig. 21.

The maximum value for the strain energy occurred in the region where the rubber backer touched the steel shoe. As the tire moved, the maximum value for the strain energy followed the center of the wheel. The load from the weight had a much larger impact than the tensile load in the track. Also, this high value of strain energy was found in the track's rubber but not in the wheel's rubber.

The rubber material properties applied at the rubber backer and the road wheel have a large impact on the stress and ESEDEN. For this analysis, the ESEDEN values for the rubber backer ranged from 50-100 psi depending on the time step of the analysis. The boundary conditions applied to the model also have a large impact on the results. Further studies will be performed to understand the effects of different parameters on the strain energy.

5. CONCLUSION REMARKS AND FUTURE WORKS

The temperature distribution of a steady-rolling tire was evaluated using a developed finite element approach. The coupled effects of loading and velocity on the temperature fields were investigated. Increasing loading increased the strain energy density, which in turn increased the values of the highest temperature and average temperature. For the rubber material properties of this study, the variation trends of the highest temperature and average temperature with the inflation pressure vary with loadings. The high temperature area decreased and moved to the shoulder position as the inflation pressure increased. The commercial 3D thermal analysis software Radtherm was employed to analyze the average temperature of tire and the Radtherm results were verified by ABAQUS. The stress and strain energy of tracks was studied as well.

In the future works, we will study:

1. Investigate the coupled influences of Young's modulus of body-ply, rubber material properties, and operational parameters (P, V, F). This includes the substitution of the standard Mooney-Rivlin model for a more advanced internal state variable model recently developed in our group.
2. Another set of more accurate material properties of tracks will be used. Material constants identified by the army will be applied to this standard model, and material properties used in an ABAQUS/Explicit model will be incorporated in an explicit, dynamic model. The boundary conditions need to be verified. Another improvement would be to run the analysis using a dynamic solver in either ABAQUS/Standard or ABAQUS/Explicit. Also, the final objective would be to determine the strain energy density for various loads and velocities. After finding the strain energy, the heat rate can be calculated and a correlation function developed for input into Radtherm.

Acknowledgements

This work was funded by the U.S. Army Tank-Automotive Research, Development & Engineering Center under contract number W56HZV-08-C-0236. The authors appreciate the contributions to this work by former colleague Dr. Liang Wang, now at Caterpillar Inc. The Center for Advanced Vehicular Systems (CAVS) acknowledges the collaboration provided through the SIMULIA Research & Development program under which licenses of ABAQUS were provided.

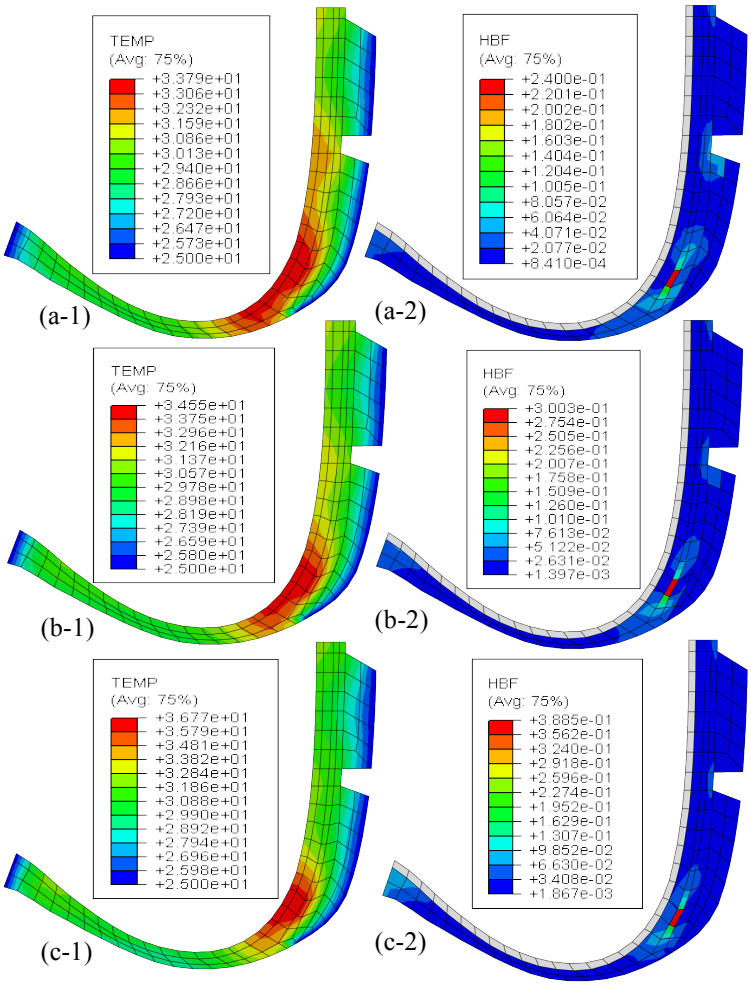

Fig. 8. Contour plots of temperature distributions and the corresponding body heat flux obtained at various inflation pressure **P** but constant loading **F**=3 kN. (a-1) temperature field at **P**=35 psi; (a-2) body heat flux distribution at P=35 psi; (b-1) temperature field at **P**=50 psi; (b-2) body heat flux distribution at **P**=50 psi; (c-1) temperature field at **P**=70 psi; (c-2) body heat flux distribution at **P**=70 psi.

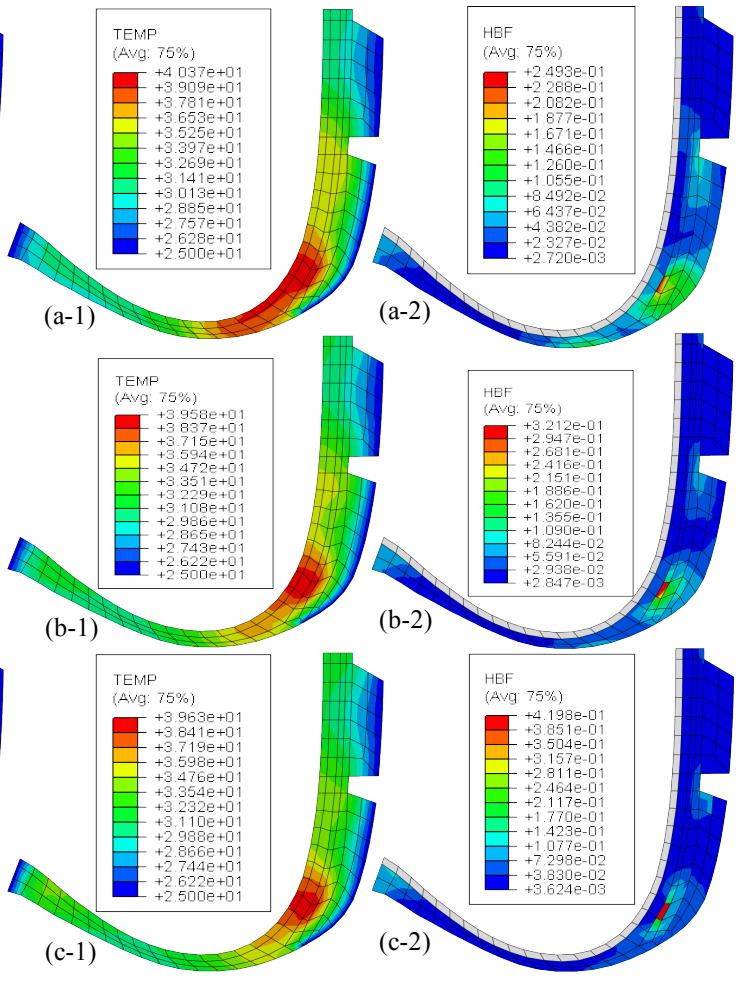

Fig. 9. Contour plots of temperature distributions and the corresponding body heat flux obtained at various inflation pressuree P but constant loading **F**=6 kN. (a-1) temperature field at **P**=35 psi; (a-2) body heat flux distribution at **P**=35 psi; (b-1) temperature field at **P**=50 psi; (b-2) body heat flux distribution at **P**=50 psi; (c-1) temperature field at **P**=70 psi; (c-2) body heat flux distribution at P=70 psi.

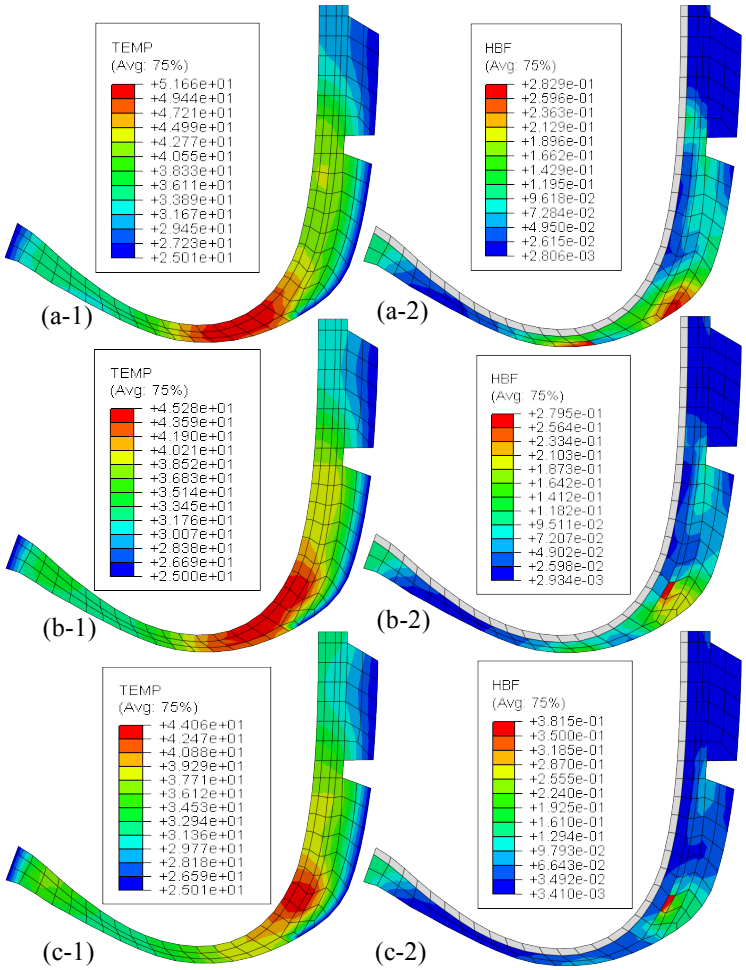

Fig. 10. Contour plots of temperature distributions and the corresponding body heat flux obtained at various inflation pressure **P** but constant loading **F**=9 kN. (a-1) temperature field at **P**=35 psi; (a-2) body heat flux distribution at **P**=35 psi; (b-1) temperature field at **P**=50 psi; (b-2) body heat flux distribution at **P**=50 psi; (c-1) temperature field at **P**=70 psi; (c-2) body heat flux distribution at **P**=70 psi.

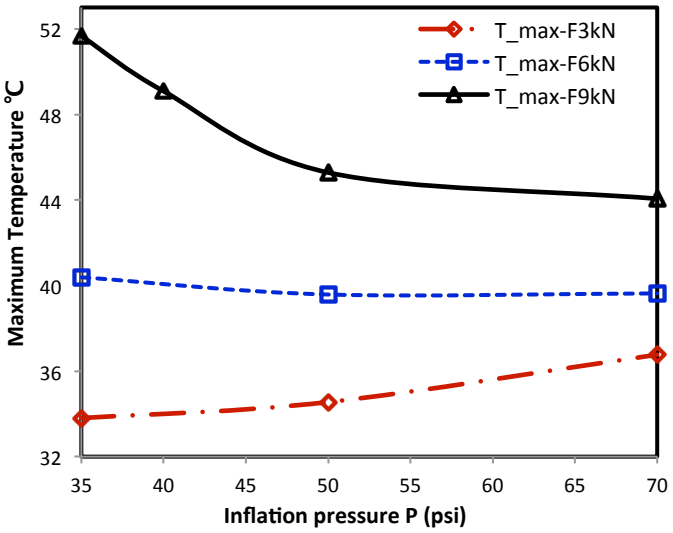

Fig. 11. The variation of maximum temperature with the inflation pressures and loadings.

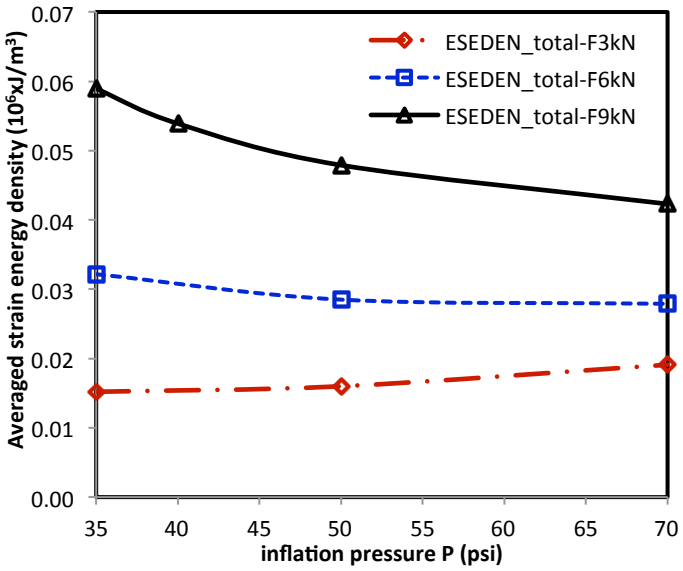

Fig. 12. The variation of the total averaged strain energy density with the inflation pressures and loadings.

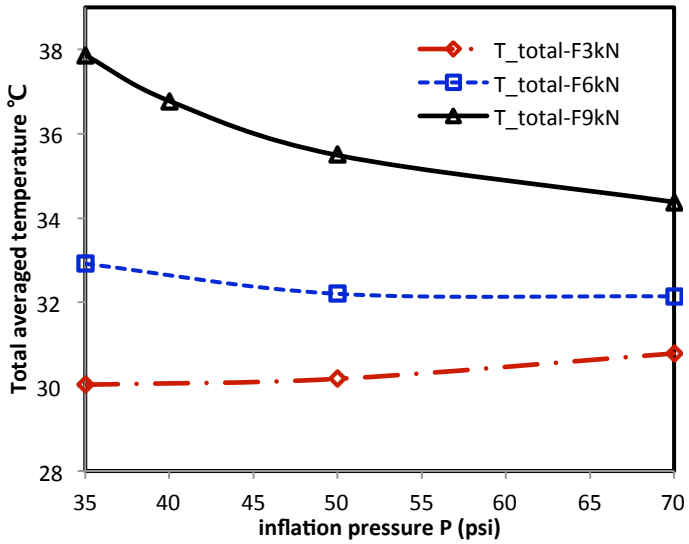

Fig. 13. The variation of the total averaged temperature with the inflation pressures and loadings.

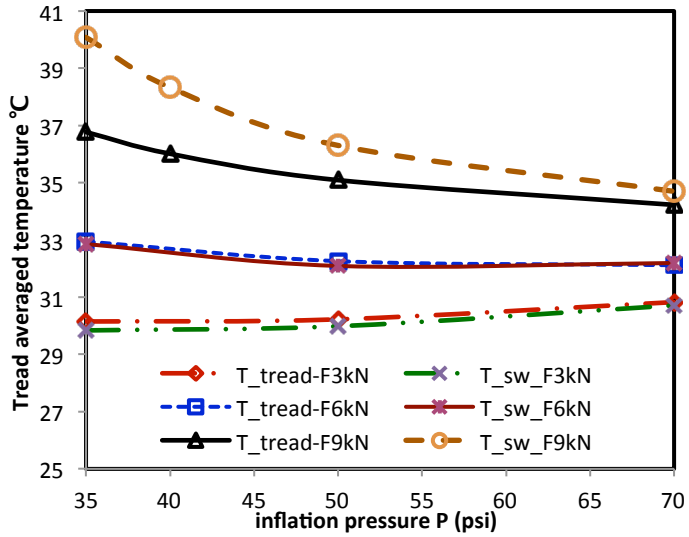

Fig. 14. The variation of the average temperature of the tread (T_tread) and sidewall (T_sw) with the inflation pressures and loadings.

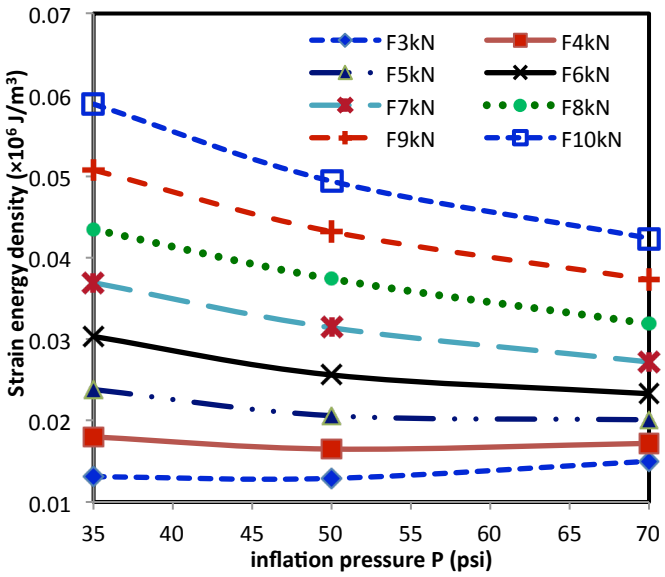

Fig. 15. The variation of the averaged strain energy density of tread ($\overline{ESE}_{Tread}$) with the inflation pressures and loadings.

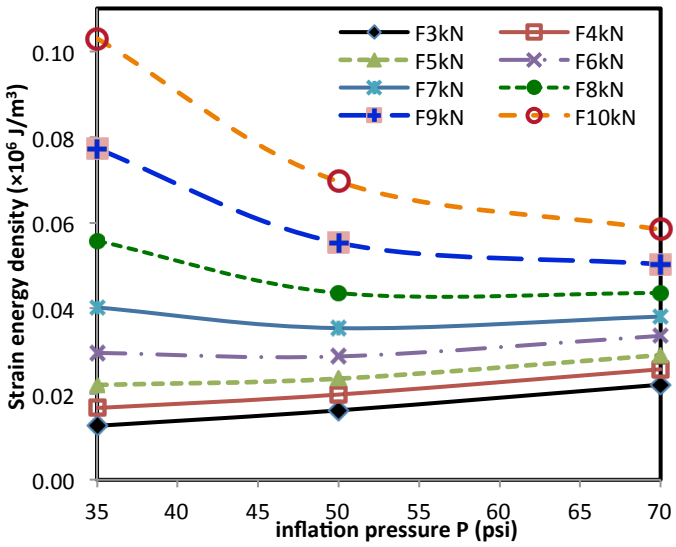

Fig. 16. The variation of the averaged strain energy density of tread ($\overline{ESE}_{sidewall}$) with the inflation pressures and loadings.

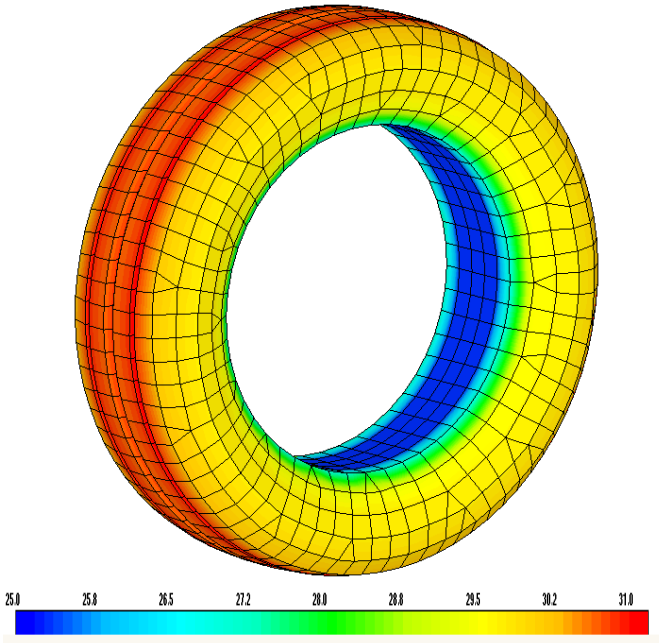

Fig. 17. Contour plot of average temperature of the tread and sidewall of a steady-state rolling tire at **P**=35 psi, **V**= 80 km/h, **F**=3kN.

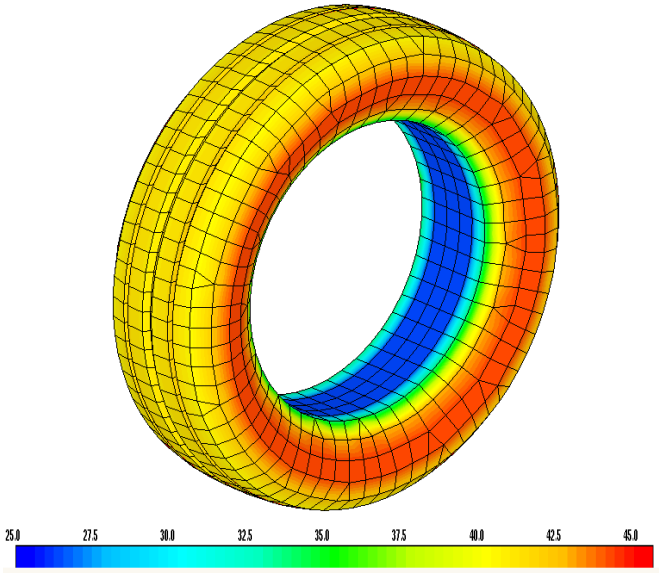

Fig. 18. Contour plot of average temperature of the tread and sidewall of a steady-state rolling tire at **P**=35 psi, **V**= 80 km/h, **F**=9kN.

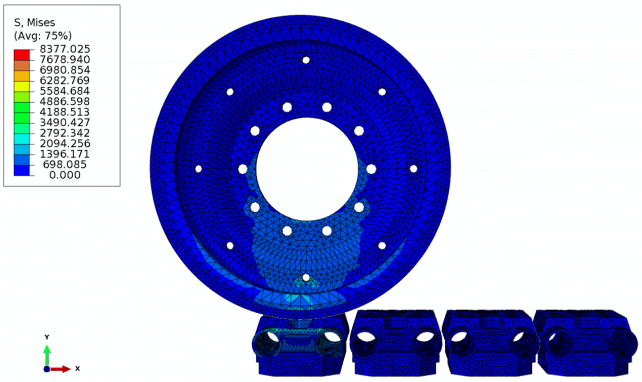

Fig. 19. Stress from the loading step.

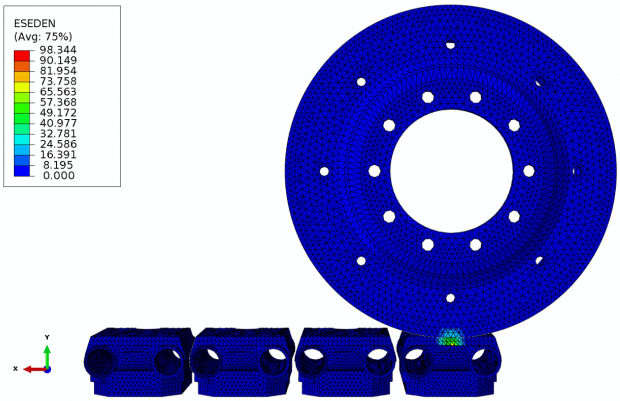

Fig. 20. ESEDEN at the beginning of rolling.

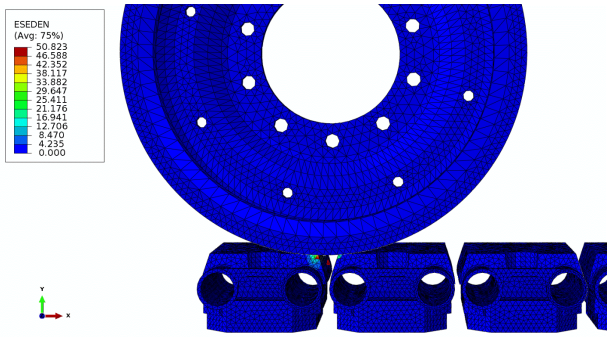

Fig. 21. ESEDEN at the transition of pads.

Table 4. The averaged strain energy density of tread ($\overline{ESE}_{Tread}$) and sidewall ($\overline{ESE}_{Sidewall}$) calculated at various inflation pressure **P**, velocity **V**, and loading **F**.

P (psi)	**V** (km/h)	**F** (kN)	$\overline{ESE}_{Tread}$ ($\times 10^6$ J/m^3)	$\overline{ESE}_{Sidewall}$ ($\times 10^6$ J/m^3)
35	40	3	1.31E-02	1.26E-02
50	40	3	1.29E-02	1.62E-02
70	40	3	1.50E-02	2.22E-02
35	60	3	1.41E-02	1.28E-02
50	60	3	1.41E-02	1.61E-02
70	60	3	1.63E-02	2.19E-02
35	80	3	1.58E-02	1.32E-02
50	80	3	1.59E-02	1.62E-02
70	80	3	1.83E-02	2.17E-02
35	40	4	1.80E-02	1.67E-02
50	40	4	1.65E-02	1.99E-02
70	40	4	1.72E-02	2.58E-02
35	60	4	1.91E-02	1.68E-02
50	60	4	1.77E-02	1.98E-02
70	60	4	1.86E-02	2.56E-02
35	80	4	2.08E-02	1.71E-02
50	80	4	1.96E-02	1.99E-02
70	80	4	2.05E-02	2.53E-02
35	40	5	2.38E-02	2.19E-02
50	40	5	2.06E-02	2.39E-02
70	40	5	2.01E-02	2.97E-02
35	60	5	2.49E-02	2.20E-02
50	60	5	2.18E-02	2.37E-02
70	60	5	2.15E-02	2.94E-02
35	80	5	2.66E-02	2.21E-02
50	80	5	2.35E-02	2.36E-02
70	80	5	2.35E-02	2.91E-02
35	40	6	3.03E-02	2.96E-02
50	40	6	2.56E-02	2.88E-02
70	40	6	2.33E-02	3.36E-02
35	60	6	3.14E-02	2.94E-02
50	60	6	2.68E-02	2.85E-02
70	60	6	2.46E-02	3.32E-02
35	80	6	3.31E-02	2.94E-02
50	80	6	2.85E-02	2.83E-02
70	80	6	2.65E-02	3.28E-02
35	40	7	3.69E-02	4.02E-02
50	40	7	3.14E-02	3.54E-02
70	40	7	2.72E-02	3.81E-02
35	60	7	3.80E-02	4.00E-02
50	60	7	3.25E-02	3.50E-02
70	60	7	2.84E-02	3.76E-02
35	80	7	3.97E-02	3.98E-02
50	80	7	3.43E-02	3.46E-02
70	80	7	3.03E-02	3.70E-02
35	40	8	4.35E-02	5.58E-02
50	40	8	3.74E-02	4.36E-02
70	40	8	3.19E-02	4.36E-02
35	60	8	4.46E-02	5.56E-02
50	60	8	3.86E-02	4.31E-02
70	60	8	3.32E-02	4.30E-02
35	80	8	4.64E-02	5.53E-02
50	80	8	4.03E-02	4.25E-02
70	80	8	3.51E-02	4.23E-02
35	40	9	5.08E-02	7.72E-02
50	40	9	4.32E-02	5.53E-02
70	40	9	3.73E-02	5.03E-02
35	60	9	5.20E-02	7.66E-02
50	60	9	4.44E-02	5.46E-02
70	60	9	3.85E-02	4.96E-02
35	80	9	5.40E-02	7.59E-02
50	80	9	4.62E-02	5.39E-02
70	80	9	4.05E-02	4.87E-02
35	40	10	5.89E-02	1.03E-01
50	40	10	4.94E-02	6.96E-02
70	40	10	4.24E-02	5.84E-02
35	60	10	6.02E-02	1.02E-01
50	60	10	5.07E-02	6.89E-02
70	60	10	4.37E-02	5.76E-02
35	80	10	6.22E-02	1.00E-01
50	80	10	5.27E-02	6.82E-02
70	80	10	4.57E-02	5.65E-02

Table 5. Average temperature of the tread and sidewall calculated by ABAQUS and Radtherm at various operational parameters including inflation pressure **P** (psi), velocity **V** (km/h), and loading **F** (kN).

	Abaqus	Radtherm	Abaqus	Radtherm
Operational parameters	Tread T_avg	Tread T_avg	Sidewall T_avg	Sidewall T_avg
P35V80F3	30.1493	30.78	29.84	29.84
P50V80F3	30.2262	30.74	29.98498	30.56
P70V80F3	30.8282	31.1	30.71416	31.57
P35V80L6	32.9472	33.61	32.85517	33.12
P50V80F6	32.2597	33.13	32.09213	32.91
P70V80F6	32.1184	32.94	32.19529	33.13
P35V80F9	36.0126	38.48	38.32890	41.38
P50V80F9	35.0906	37.49	36.30263	39.06
P70V80F9	34.2255	36.4	34.69769	37.83

REFERENCES

[1] T. G. Ebbott, R. L. Hohman, J. P. Jeusette, V. Kerchman,"Tire Temperatureand Rolling Resistance Prediction with Finite Element Analysis," *Tire Sci Technol*, Vol. 27, 1999, pp. 2-21.

[2] Wong, J. Y., *Theory of Ground Vehicles*, 3rd Ed., Wiley, 2001.

[3] Lin, Y. -J., Hwang, S. –J., "Temperature Prediction of Rolling Tires by Computer Simulation," *Math Comput Simulat*, Vol. 67, 2004, pp. 235-249.

[4] "An Integrated Approach for Transient Rolling of tires," *Abaqus Technology Brief*, 2007.

[5] User manual of Radtherm Version 10.2, 2012